RESEARCH ARTICLE

Micropolar Fluid Flows Past a Porous Shell: A Model for Drug Delivery Using Porous Microspheres

Curtis Boodoo*

ABSTRACT

The creeping flow of an incompressible, bounded micropolar fluid past a porous shell is investigated. The porous shell is modeled using a Darcy equation, sandwiched between a pair of transition Brinkman regions. Analytical expressions for the stream function, pressure, and microrotations are given for each region. Streamline patterns are presented for variations in hydraulic resistivity, micropolar constants, porous layer thickness, and Ochoa-Tapia stress jump coefficient. An expression for the dimensionless drag for the unbounded case of the system is presented, and its variation with hydraulic resistivity and porous shell thickness is presented. The unbounded case represents a theoretical model for oral drug delivery using porous microspheres. It was found that optimal circulation between the porous region and the outer fluid occurred for low values of hydraulic resistivity and for a complete porous sphere.

Keywords: Micropolar fluid, Oral drug delivery, Porous media, Spherical shell.

1. INTRODUCTION

Controlled release drug delivery employs drug-encapsulating devices from which therapeutic agents may be released at controlled rates for long periods of time, ranging from days to months. Such systems offer numerous advantages over traditional methods of drug delivery, including tailoring of drug release rates, protection of fragile drugs, and increased patient comfort and compliance. Porous microspheres are ideal vehicles for many controlled delivery applications due to their ability to encapsulate a variety of drugs, biocompatibility, high bioavailability, and sustained drug release characteristics. The types of microspheres used in controlled drug delivery include Bioadhesive, Magnetic, Floating, Radioactive, and Polymeric Microspheres.

Considerable work has been carried out on micropolar fluids since the introduction of its theory [1]. Micropolar fluids represent fluids consisting of rigid, randomly oriented bar-like elements or dumbbell-shaped molecules. Each volume element has microrotation about its centroid, in addition to its translatory motion in an average sense. Micropolar fluids exhibit some microscopic effects arising from the local structure and micromotion of the fluid elements, and they can sustain a couple of stresses. Animal blood, liquid crystals, and certain polymeric fluids are a few examples of fluids that may be represented by the mathematical model of micropolar fluids.

Rao and Rao [2] discussed the creeping flow of micropolar fluid past a sphere. A more general result for Stokes flow in a micropolar fluid in the case of axisymmetric bodies has been given by Ramkissoon and Majumdar [3]; they presented an expression for the drag and applied it to the specific case of a sphere.

Bhatt [4] examined the creeping flow of a micropolar fluid produced by the relative motion of solid sphere and an inner porous sphere. His work extends Cunningham [5] work to micropolar fluids with a porous inner sphere. He obtained an expression for the force exerted on the inner porous sphere using stream functions.

Srinivasacharya and Rajyalakshmi [6] investigated creeping flow of an incompressible micropolar fluid past a porous sphere in an unbounded fluid. They used Brinkmans equation for the porous region. The boundary conditions used were the continuity of velocity, pressure, and tangential stresses across the fluid, porous region interface. They implemented a no-spin condition for the microrotation components in both regions. They presented stream function and pressure expressions for the different

regions and also gave an expression for the drag on the sphere.

Saad [7] considered the creeping asymmetric translational motion of a spheroid particle in an unbounded micropolar fluid. He also considered the motion of a spheroidal particle at the instant it passes the center of a spherical envelope filled with a micropolar fluid. He presented analytical expressions for the stream function and microrotation components obtained to first order in the small parameter characterizing the deformation. He also presented drag expressions for both the unbounded fluid and spherical envelope case.

Hoffmann *et al.* [8] investigated Stokes formula for the drag on a sphere moving with constant velocity in a micropolar fluid. A non-homogeneous boundary condition for the microrotation vector is used. They compare their expression for the drag with other authors.

Goharzadeh *et al.* [9] experimentally looked at the flow in the vicinity of a permeable interface using Particle Image Velocimetry (PIV) and Refractive Index Matching (RIM). They found from observing the average velocity profile that the horizontal velocity profile decreases continuously when moving downward from the fluid into the porous layer. Their experimental data indicates the existence of a transition layer, which is characterized by a drastic decrease in velocity. The length scale of the transition layer was found to be of the order of the grain diameter of the porous particle and much larger than the square root of the permeability, as was originally suggested by Neale and Nader [10]. They stated that a Brinkman transition layer would have a drastic decrease in fluid particle velocity and that the fluid particles then attain an average constant velocity in the porous region as predicted by the Darcy equation.

Stability analysis has also been performed on a porous medium modeled as a transition Brinkman layer overlying a Darcy layer. Hill and Straughan [11] examined a three (3) layer configuration comprising a clear fluid overlying a transition Brinkman layer, which in turn overlies a Darcy porous layer. These three (3) layers configuration was used to numerically investigate the instability of Poiseuille flow. They found two (2) modes of instability corresponding to the fluid and porous layers, respectively. They found that the stability characteristics of the system are influenced by the depth ratio between the porous and fluid layers and the transition layer depth.

The intent of the problem is to investigate the hydrodynamics associated with a porous polymer cell, geometrically modeled as a porous microsphere, that is orally administered as a drug carrier for a sustained drug delivery system to treat colon cancer. A porous spherical shell is used to generalize the geometry, and micropolar fluid is used to model the complex Non-Newtonian fluid present in the colon. Creeping axisymmetric flow of an incompressible micropolar fluid past a porous shell is considered. The porous region is modeled using Darcy equation sandwiched between two transition Brinkman regions. A stream function formulation is used to solve the system. The accompanying boundary conditions used are continuity of velocity, normal and tangential stresses, and non homogeneous microrotations across the fluid porous region interfaces. At the Brinkman- Darcy interfaces, continuity of velocity, normal stresses, microrotations, and the Beavers and Joseph condition are implemented. Plots of the stream functions as they vary with hydraulic resistivity, micropolar coupling parameter, tangential stress jump parameter, and the thickness of the porous shell are presented and discussed. An analytical expression for the dimensionless drag, in the unbounded fluid case, is derived, and plots of the dimensionless drag as it varies with hydraulic resistivity and porous layer thickness are presented. The results presented by Ramkissoon and Majumdar [3] are also recovered from the model.

2. Model Formulation

We consider the case of a steady, creeping, axisymmetric, incompressible micropolar fluid flow past a porous shell. (r, θ, ϕ) denote the spherical polar coordinate system, with the corresponding unit base vectors $(\vec{e}_r, \vec{e}_\theta, \vec{e}_\phi)$ with scale factors $(h_1, h_2, h_3) = (1, r, r \sin \theta)$.

The ambient velocity V defined at a finite radius $r = r_e$ is upward and parallel to the polar z-axis. The porous shell has internal radius $r = b$ and external radius $r = a$. The porous regions, in Fig. 1, is modeled as two transition Brinkman layers separated by a Darcy region. The thickness of the transition Brinkman layers ϵ, is given [6]:

$$\epsilon = 0.1 \left(1 - \frac{b}{a} \right) \tag{1}$$

The velocity vector $\vec{q}^{(i)}$ and micro rotation vector $\vec{\omega}^{(i)}$ associated with the micropolar fluid flow is given by:

$$\vec{q}^{(i)} = \begin{pmatrix} q_r^{(i)} & (r, \theta) \\ q_\theta^{(i)} & (r, \theta) \\ 0 \end{pmatrix} \quad \text{and} \quad \vec{\omega}^{(i)} = \begin{pmatrix} 0 \\ 0 \\ \omega_\phi^{(i)} (r, \theta) \end{pmatrix} \tag{2}$$
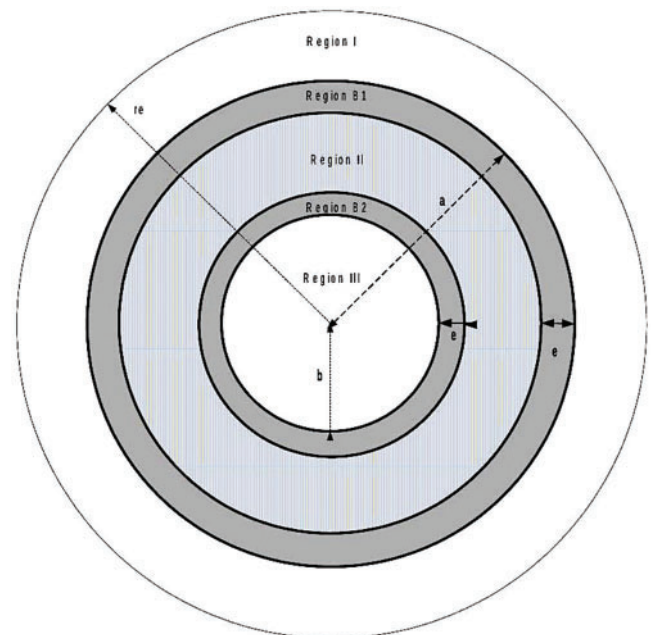

Fig. 1. Different regions: Region I—Outer fluid region, Region III—Inner fluid region, Region II—Darcy region, Region B1 and B2—Brinkman regions.

For axisymmetric flow, Stokes Stream functions $\Psi^{(i)}$ in spherical polar coordinates is given for $i = 1, 2, 3, b1$ and $b2$:

$$q_r^{(i)} = -\frac{1}{r^2 \sin\theta} \frac{\partial}{\partial\theta} \Psi^{(i)} \text{ and } q_\theta^{(i)} = \frac{1}{r\sin\theta} \frac{\partial}{\partial r} \Psi^{(i)} \quad (3)$$

2.1. Region I and Region III

Region I consists of micropolar fluid outside the porous sphere, and Region III consists of micropolar fluid inside the inner radius of the shell, $0 \leq r \leq b$. The governing equations for a steady flow of an incompressible micropolar fluid under Stokesian assumption in the absence of body force and body coupling is given by Srinivasacharya and Rajyalakshmi [12]. For $i = 1$ and 3:

$$\nabla \cdot \vec{q}^{(i)} = 0$$
$$-\nabla p^{(i)} - (\mu + \kappa)\left(\nabla \times \nabla \times \vec{q}^{(i)}\right) + \kappa \nabla \times \vec{\omega}^{(i)} = 0$$
$$-2\kappa\vec{\omega}^{(i)} + \kappa\nabla \times \vec{q}^{(i)} - \gamma\nabla \times \nabla \times \vec{\omega}^{(i)} \quad (4)$$
$$+ (\alpha_m + \beta_m + \gamma)\nabla\left(\nabla \cdot \vec{\omega}^{(i)}\right) = 0$$

where $\vec{q}(i)$ is the velocity vectors, p(i) is fluid pressure, $\vec{w}(i)$ is microrotation vector, μ, κ , γ , αm and βm is micropolar constants.

The micropolar constants κ, γ, α_m and β_m satisfy the following inequalities:

$$2\mu + \kappa \geq 0, \ \kappa \geq 0, \ 3\alpha_m + \beta_m + \gamma \geq 0 \text{ and } \gamma \geq |\beta_m| \quad (5)$$

2.2. Region B1 and B2

Region B1, $a - \epsilon \leq r \leq a$ and Region B2, $b \leq r \leq b + \epsilon$ are both modeled as a thin transitional Brinkman porous layer of thickness ϵ, where $\epsilon = 0.1(1 - b/a)$ [6]. The governing equations are given by Srinivasacharya and Rajyalakshmi [13]. For $i = b1$ and $b2$:

$$\nabla \cdot \vec{q}^{(i)} = 0$$
$$\frac{\mu}{k}\vec{q}^{(i)} + \nabla p^{(i)} - \kappa\nabla \times \vec{\omega}^{(i)} + (\mu + \kappa)\left(\nabla \times \nabla \times \vec{q}^{(i)}\right) = 0$$
$$-2\kappa\vec{\omega}^{(i)} + \kappa\nabla \times \vec{q}^{(i)} - \gamma\nabla \times \nabla \times \vec{\omega}^{(i)} \quad (6)$$
$$+ (\alpha_m + \beta_m + \gamma)\nabla\left(\nabla \cdot \vec{\omega}^{(i)}\right) = 0$$

2.3. Region II

Region II, $b + \epsilon \leq r \leq a - \epsilon$ is modeled as a Darcy porous region. The governing equations are given by Sharma and Gupta [14]:

$$\nabla \cdot \vec{q}^{(2)} = 0$$
$$\frac{1}{k}(\mu + \kappa)\vec{q}^{(2)} + \kappa\nabla \times \omega^{(2)} = \nabla p^{(2)}$$
$$-2\kappa\omega^{(2)} + \kappa\nabla \times \vec{q}^{(2)} - \gamma\nabla \times \left(\nabla \times \omega^{(2)}\right) \quad (7)$$
$$+ (\alpha + \beta + \gamma)\nabla\left(\nabla \cdot \omega^{(2)}\right) = 0$$

2.4. Dimensionless Form of the Governing Equations

A dimensionless analysis is performed on the governing equations for all the regions. The dimensionless variables

$\psi^{(i)}, p^{(i)*}, r^*, \omega_\phi^{*(i)}, q_{r*}^{(i)}, q_\theta^{(i)*}$ and α^2 are defined as follows:

$$\Psi^{(i)} = a^2 V\psi^{(i)}, \quad p^{(i)} = \frac{\mu}{a} Vp^{(i)*}, \quad r = ar^*,$$
$$\omega_\phi^{(i)}(r,\theta) = \frac{V}{a}\omega_\phi^{*(i)}(r,\theta) \quad (8)$$
$$q_r^{(i)} = Vq_{r*}^{(i)*}, \quad q_\theta^{(i)} = Vq_\theta^{(i)*} \text{ and } \alpha^2 = \frac{a^2}{k}$$

where α^2 is the hydraulic resistivity of the brinkman porous region and i is 1 and 3.

The dimensionless variables are substituted into the governing equations and for simplicity, the superscript (*) is removed.

The governing equations in dimensionless form for the various regions are given by Region I and III ($i = 1$ and 3):

$$\frac{1}{2}\left(E^2\psi^{(i)} + \frac{2-N}{Nm^2}E^4\psi^{(i)}\right) = r\sin\theta\omega_\phi^{(i)} \quad (9)$$
$$E^4\left(E^2 - m^2\right)\psi^{(i)} = 0$$

Region B1 and B2 ($i = b1$ and $b2$):

$$\omega_\phi^{(i)} = \frac{1}{2r\sin\theta}E^2\psi^{(i)}$$
$$+ \frac{1}{2r\sin\theta}\left(\frac{2-N}{m^2}\right)E^2\left(r\sin\theta\omega_\phi^{(i)}\right) \quad (10)$$
$$0 = E^2\left(E^2 - \chi^2\right)\left(E^2 - \varrho^2\right)\psi^{(i)}$$

Region II:

$$r\sin\theta\omega_\phi^{(2)} = -\frac{1}{2}\left(1 + \alpha^2\left(\frac{2-N}{Nm^2}\right)\right)E^2\psi^{(2)}$$
$$E^4\psi^{(2)} - \left(\frac{2\alpha^2m^2}{\alpha^2(2-N) + Nm^2}\right)E^2\psi^{(2)} = 0 \quad (11)$$

where

$$\varrho^2 = \frac{1}{2}\left(\alpha^2(1-N) + m^2\right)$$
$$+ \frac{\alpha}{2}\sqrt{\alpha^2\left((1-N) + \frac{m^2}{\alpha^2}\right)^2 - \frac{8m^2(1-N)}{2-N}}$$
$$\chi^2 = \frac{2m^2\alpha^2(1-N)}{(2-N)\varrho^2} \quad (12)$$
$$E^2 = \frac{\partial^2}{\partial r^2} + \frac{1}{r^2}\frac{\partial^2}{\partial\theta^2} - \frac{\cot\theta}{r^2}\frac{\partial}{\partial\theta}$$

3. SOLUTIONS FOR THE DIFFERENT REGIONS

Solutions for Regions I and III, as well as regions B1 and B2, are given by Srinivasacharya and Rajyalakshmi [13] as:

$$\psi^{(i)} = \left[A^{(i)}r^2 + \frac{B^{(i)}}{r} + C^{(i)}r^4 + D^{(i)}r + E^{(i)}\sqrt{r}K_{\frac{3}{2}}(mr) \right.$$
$$\left. + F^{(i)}\sqrt{r}I_{\frac{3}{2}}(mr) \right] \frac{\sin^2\theta}{2}$$

$$\omega_\phi^{(i)} = \frac{\sin\theta}{2N} \left(m^2\sqrt{r}F^{(i)}I_{\frac{3}{2}}(mr) + m^2\sqrt{r}E^{(i)}K_{\frac{3}{2}}(mr) \right.$$
$$\left. + 5NC^{(i)}r - \frac{N}{r^2}D^{(i)} \right)$$

(13)

where $i = 1$ and 3 and

$$\psi^{(i)} = \left[A^{(i)}r^2 + \frac{B^{(i)}}{r} + C^{(i)}\sqrt{r}K_{\frac{3}{2}}(\chi r) \right.$$
$$+ D^{(i)}\sqrt{r}I_{\frac{3}{2}}(\chi r) + E^{(i)}\sqrt{r}K_{\frac{3}{2}}(\varrho r)$$
$$\left. + F^{(i)}\sqrt{r}I_{\frac{3}{2}}(\varrho r) \right] \frac{\sin^2\theta}{2}$$

(14)

$$\omega_\phi^{(i)} = -\frac{\sin\theta}{4Nm^2r^{\frac{9}{2}}} \left(\tilde{C}\left(C^{(i)}\right) + \tilde{D}\left(D^{(i)}\right) \right.$$
$$\left. + \tilde{E}\left(E^{(i)}\right) + \tilde{F}\left(F^{(i)}\right) \right)$$

where $i = b1$ and $b2$ and:

$$\tilde{C} = r^4\chi^2 \left((N-2)\chi^2 + \alpha^2(N-2)(N-1) \right.$$
$$\left. -Nm^2 \right) K_{\frac{3}{2}}(\chi r)$$
$$\tilde{D} = r\chi^2 \left((N-2)\chi^2 + \alpha^2(N-2)(N-1) \right.$$
$$\left. -Nm^2 \right) I_{\frac{3}{2}}(\chi r)$$
$$\tilde{E} = r\varrho^2 \left((N-2)\chi^2 + \alpha^2(N-2)(N-1) \right.$$
$$\left. -Nm^2 \right) K_{\frac{3}{2}}(\varrho r)$$
$$\tilde{F} = r^4\varrho^2 \left((N-2)\chi^2 + \alpha^2(N-2)(N-1) \right.$$
$$\left. -Nm^2 \right) I_{\frac{3}{2}}(\varrho r)$$

(15)

Following the analysis given by Happel and Brenner [5], the solutions for Region II is given by:

$$\psi^{(2)} = \left(A^{(2)}r^2 + \frac{B^{(2)}}{r} + E^{(2)}\sqrt{r}Y_{\frac{3}{2}}(m_d r) \right.$$
$$\left. + F^{(2)}\sqrt{r}J_{\frac{3}{2}}(m_d r) \right) \frac{\sin^2\theta}{2}$$

$$\omega_\phi^{(2)} = -\frac{\left(\alpha^2(N-2) - Nm^2\right)m_d^2}{4Nm^2} \left(\frac{\sin\theta}{r^{\frac{1}{2}}} \right)$$
$$\times \left(E^{(2)}Y_{\frac{3}{2}}(m_d r) + F^{(2)}J_{\frac{3}{2}}(m_d r) \right)$$

(16)

where

$$m_d^2 = \left(\frac{2\alpha^2m^2}{\alpha^2(2-N) + Nm^2} \right)$$

(17)

where $K_{3/2}(mr)$-modified Bessels function of the first kind of order 3/2, $I_{3/2}(mr)$-modified Bessels function of the second kind of order 3/2, $Y_{3/2}(m_d r)$-Bessels function of the second kind of order 3/2, $J_{3/2}(m_d r)$-Bessels function of the first kind of order 3/2, and $A^{(i)}, B^{(i)}, C^{(i)}, D^{(i)}, E^{(i)}$ and $F^{(i)}$ represents the constants for the different regions, specified by the superscript (i).

3.1. Dimensionless Boundary Conditions

The following dimensionless boundary conditions are used to obtain the twenty-five (25) total constants present in the general solutions for all the regions:

1. The radial velocity $q_r^{(3)}$ and tangential velocity $q_\theta^{(3)}$ are finite at $r = 0$.
2. The radial and tangential velocity fields are defined at $r = \frac{r_e}{a}$:

$$q_r^{(1)} = \cos\theta \quad \text{and} \quad q_\theta^{(1)} = -\sin\theta$$

3. The microrotations $\omega^{(i)}$ is equal to the vorticity of the micropolar fluid at $r = \frac{r_e}{a}$, $r = 1$ and $r = r_3 = b/a$:

$$\omega^{(i)} = \alpha_2\nabla \times \vec{q}^{(1)} \text{ where } 0 \leq \alpha_2 \leq 1 \text{ and } i = 1, 3$$

and $b1$.
4. Continuity of both radial q_r and tangential q_θ velocity components at $r = 1, r = r_1 = 1 - \epsilon, r = r_2 = b/a + \epsilon$ and $r = r_3 = b/a$.
5. Continuity of normal stresses at $r = 1, r = r_1 = 1 - \epsilon, r = r_2 = b/a + \epsilon$ and $r = r_3 = b/a$.
6. Ochoa-Tapia jump in tangential Stress Jump condition at $r = 1$ and $r = r_3 = b/a$.
7. The micro-rotations $\omega^{(i)}$ are equal at $r = r_1 = 1 - \epsilon$ and $r = r_2 = b/a + \epsilon$.
8. Beavers and Joseph boundary condition at $r = r_1 = 1 - \epsilon$ and $r = r_2 = b/a + \epsilon$.

The solutions for the different regions given by (15)–(20), along with the dimensionless boundary conditions above, are used to obtain the constants and uniquely solve the system.

4. RESULTS

4.1. Streamline Patterns

The streamline patterns are displayed in spherical polar coordinates (r and ϕ) with the outline of the porous shell in red. The direction of the velocity V is upwards.

4.1.1. Streamline Patterns for Varying Hydraulic Resistivity α

- Streamline patterns for varying hydralic resistivity Fig. 2.
- Streamline patterns for varying porous lauer thickness Fig. 3.

4.1.2. Streamline Patterns for Varying Porous Layer Thickness ε_p

4.2. Drag for the Unbounded Fluid Case

For unbounded micropolar fluid flow past a porous shell the boundary conditions remain the same as for the bounded system, except that the three (3) boundary conditions at $r = r_e$ are now excluded.

The stream function $\hat{\psi}^{(1)}$ corresponding to the unbounded case is given by:

$$\hat{\psi}^{(1)} = \left(r^2 + \frac{\hat{B}^{(1)}}{r} + \hat{D}^{(1)}r + \hat{E}^{(1)}\sqrt{r}K_{\frac{3}{2}}(mr) \right) \frac{\sin^2\theta}{2}$$

(18)

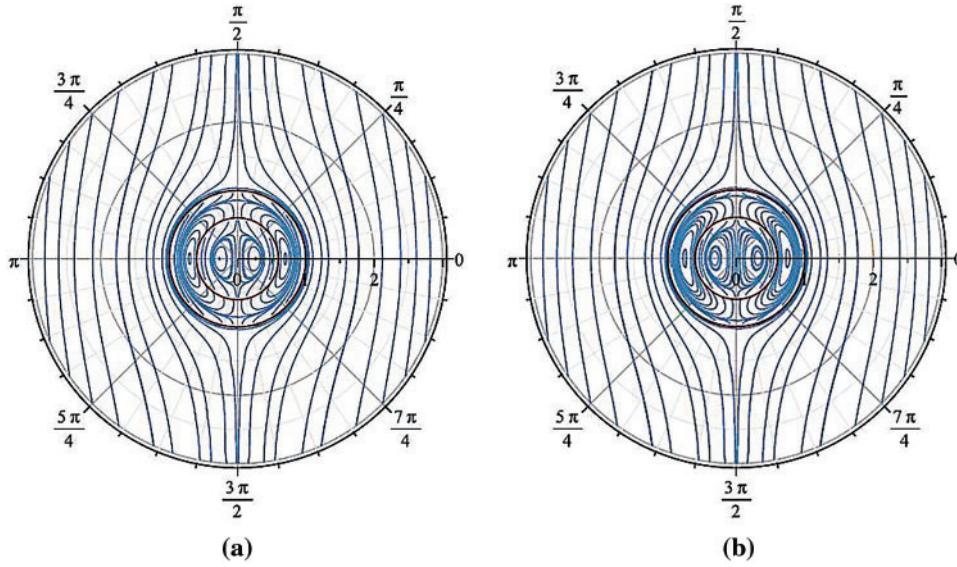Fig. 2. Streamline patterns for varying α: (a) $\alpha = 5$ and (b) $\alpha = 7$, b/a = 0.6, $\alpha_j = 1.45$, $\beta = 1/2$, N = 0.5 and m = 20.
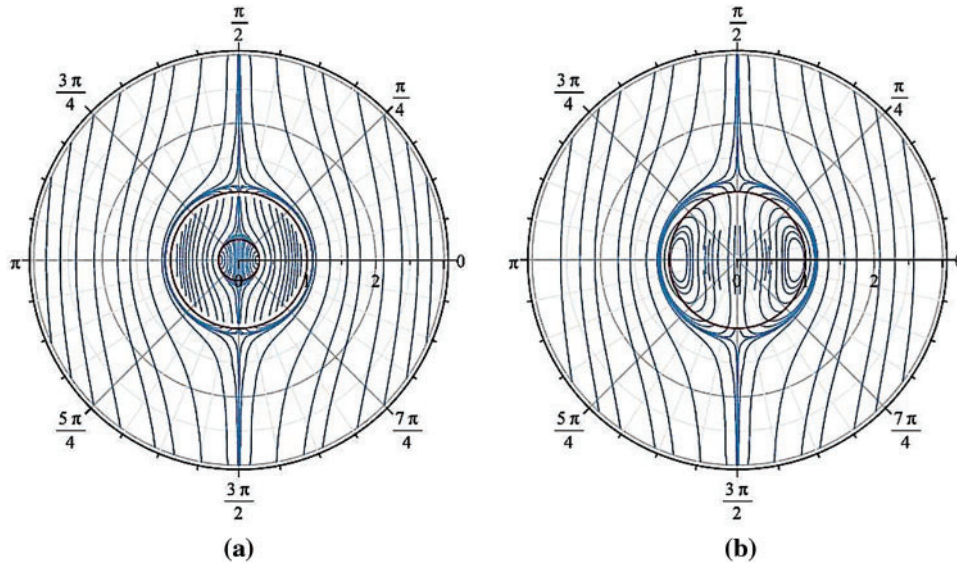

Fig. 3. Streamline patterns for: (a) $\varepsilon_p = 0.7$, $\alpha = 2$, b/a = 0.6, $\alpha_j = 1.45$, $\beta = 0.5$, m = 20 and N = 0.5, (b) $\varepsilon_p = 0.99$, $\alpha = 2$, b/a = 0.6, $\alpha_j = 1.45$, $\beta = 0.5$, m = 20 and N = 0.5.

The corresponding expressions for the pressure $\hat{p}^{(1)}$ and microrotation $\hat{\omega}^{(1)}$ are given by:

$$\hat{\omega}^{(1)} = -\frac{\sin\theta}{2}\left(\frac{\hat{D}^{(1)}}{r^2} - \frac{\hat{E}^{(1)}m^2 K_{\frac{3}{2}}(mr)}{N\sqrt{r}}\right)$$

$$\hat{p}^{(1)} = -\frac{(N-2)}{2(N-1)}\left(\frac{\hat{D}^{(1)}}{r^2}\right)\cos\theta \tag{19}$$

where $\hat{B}^{(1)}$, $\hat{D}^{(1)}$ and $\hat{E}^{(1)}$ are constants for the unbounded system of equations.

The drag formula for a sphere in a micropolar fluid is given by Ramkissoon and Majumdar [10]. In dimensionless form, it is given by:

$$D_l = \int_0^\pi \left[\left(-p^{(1)} + \frac{(2-N)}{(1-N)}\frac{\partial q_r^{(1)}}{\partial r}\right)\cos\theta \right.$$
$$- \left(\left(\frac{1}{r}\frac{\partial q_r^{(1)}}{\partial \theta} + r\frac{\partial}{\partial r}\left(\frac{q_\theta^{(1)}}{r}\right)\right)\right) \tag{20}$$
$$\left. + \frac{N}{(1-N)}\frac{\partial}{\partial r}q_\theta^{(1)} - \frac{N}{(1-N)}\omega^{(1)}\right)\sin\theta\Bigg]_{r=1}\sin\theta\,d\theta$$

where D_l is the dimensionless drag.

Substituting (17)–(19) into (20) gives:
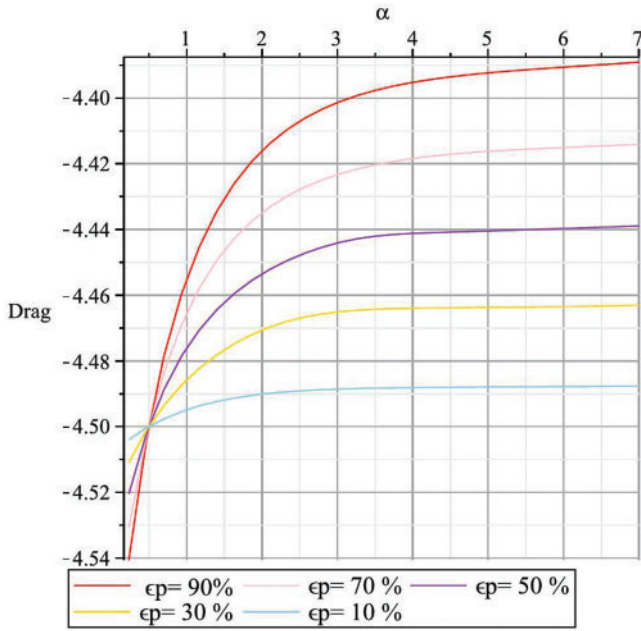
$$D_l = \frac{(N-2)}{(N-1)}\hat{D}^{(1)} \tag{21}$$

Fig. 4. Dimensionless drag against α for varying ϵ_p:$\beta = 0.5$, N $= 0.5$, m $= 10$ and $\alpha\_j = 1.4$.

5. Discussion

In Fig. 2, there are regions of closed rings on either side of the porous shell that represent fluid flow that is circulating. The greater resistance to fluid flow within the porous region causes the reflecting or bending back of particular fluid particles within the inner fluid regions, as seen in Fig. 2, resulting in trapped circulating fluid particles.

Fig. 3b has a porous region thickness that is 99% of the overall thickness of the shell, i.e., the shell can be approximated to a porous sphere, and the uniform velocity field V is defined at $r_e = 100$, this simulates unbounded fluid flow. Fig. 3b contains the Brinkman transition regions that are set to 10% of the overall thickness of the porous region [11]; hence, the porous region in Fig. 3b is primarily a Darcy region. In Fig. 3b the Brinkman regions are 99% and the Darcy region 1%, of the total porous region. The plots of Fig. 3b vary from that of [6] who looked at micropolar fluid flow past a Brinkman porous sphere. The streamline patterns from Srinivasacharya and Rajyalakshmi [6] pass straight through the porous region with very little bending of the streamlines and no circulation regions. It should be noted that the boundary conditions used by Srinivasacharya and Rajyalakshmi are different from the boundary conditions of this model. Srinivasacharya and Rajyalakshmi used continuity of pressure, tangential stresses, velocities, and homogeneous microrotations, whereas for this model, continuity of normal stresses, jump in tangential stresses, continuity of velocities, and non-homogeneous microrotations are used.

There is a decrease in dimensionless drag with increasing hydraulic resistivity α, for varying porous layer thickness ϵ_p, this is illustrated in Fig. 4. The overall decrease in drag over the range of $0 \leq \alpha \leq 7$ is greater as the porous layer thickness ϵ_p increases.

Increasing α represents a decrease in permeability. Smaller values of permeability represent a greater resistance to fluid flow within the porous regions of the shell. The greater resistance to fluid flow causes less fluid particles to enter or penetrate the outer radius of the porous shell. A decrease in fluid volume flow around the outer radius of the shell causes a decrease in the overall frictional forces exerted by the fluid on the porous shell and, hence, a decrease in drag. When the porous region thickness is increased, the effect of α on the overall system is much more significant. The increasing of α which causes a decrease in drag, now causes a much more significant decrease in drag for higher values of porous layer thickness.

The parameters of specific interest are the manufacturable porous parameters, hydraulic resistivity α and the porous layer thickness ϵ_p. These parameters, in the context of modeling sustained drug delivery, represent external parameters that can be varied.

The circulation regions, on either side of the porous shell, crosses the porous regions and enters the outer micropolar region. This effect is most significant for lower values of α. Hence for lower values of α, circulation or mixing between the porous region and the micropolar outer fluid is most pronounced. The drug stored within the porous material is most effectively mixed and delivered to the outer fluid for lower values of α.

For higher values of α however, the circulation regions are confined to inside the porous region and inner micropolar fluid region. The drug stored in the porous regions is circulated internally within the porous region and not effectively delivered to the outer micropolar fluid.

Circulation regions become more pronounced and extend into the outer micropolar fluid region for a porous layer thickness of 50% and greater. The most circulation occurs when the porous layer thickness is 99% or close to a whole porous sphere.

6. Conclusion

To ensure effective delivery of the drugs stored in the porous region, significant mixing between the porous and outer fluid regions must take place. The results show that mixing between the porous and outer fluid region is at its most pronounced for low values of α and for a whole porous sphere. Optimal drug delivery takes place when a whole porous sphere of high permeability is used as the dug carrier.

Conflict of Interest

The authors declare that they do not have any conflict of interest.

References

[1] Bhatt BS. Slow motion of a micropolar fluid through a porous sphere bounded by a solid sphere. *Proc Math Sci*. 1982, November;91(3):211–6.

[2] Cunningham E. On the velocity of steady fall of spherical particles through fluid medium. *Proc R Soc London. Series A*. 1910, March;83(563):357–65.

[3] Eringen AC. Simple microfluids. *Int J Eng Sci*. 1964, May;2(2):205–17.

[4] Goharzadeh A, Saidi A, Wang D, Merzkirc W, Khalil A. An experimental investigation of the brinkman layer thickness at a Fluid-Porous interface. In *IUTAM Symposium on One Hundred Years of Boundary Layer Research*. vol. 129, Gladwell GML, Meier GEA, Sreenivasan KR, Heinemann H, Eds. Dordrecht: Springer Netherlands, 2006, pp. 445–54.

[5] Happel J, Brenner H. *Low Reynolds Number Hydrodynamics: With Special Applications to Particulate Media*. Springer; 1983, December.

[6] Hill AA, Straughan B. Poiseuille flow in a fluid overlying a porous medium. *J Fluid Mech*. 2008;603:137–49.

[7] Hoffmann K, Marx D, Botkin ND. Drag on spheres in micropolar fluids with non-zero boundary conditions for microrotations. *J Fluid Mech*. 2007;590:319–30.

[8] Kuznetsov AV. Analytical investigation of the fluid flow in the interface region between a porous medium and a clear fluid in channels partially filled with a porous medium. *Appl Sci Res*. 1996 Mar;56(1):53–67.

[9] Neale G, Nader W. Practical significance of brinkman's extension of Darcy's law: Coupled parallel flows within a channel and a bounding porous medium. *Can J Chem Eng*. 52(4):475–8.

[10] Ramkissoon H, Majumdar SR. Drag on an axially symmetric body in the stokes flow of micropolar fluid. *Phys Fluids*. 1976 Jan;19(1):16–21.

[11] Rao SKL, Rao PB. The slow stationary flow of a micropolar liquid past a sphere. *J Eng Math*. 4(3):209–17.

[12] Saad EI. Motion of a spheroidal particle in a micropolar fluid contained in a spherical envelope. *Can J Phys*. 2008;86(9):1039–56.

[13] Srinivasacharya D, Rajyalakshmi I. Creeping flow of micropolar fluid past a porous sphere. *Appl Math Comput*. 2004 Jun;153(3):843–54.

[14] Sharma R, Gupta U. Thermal convection in micropolar fluids in porous medium. *Int J Eng Sci*. 1995 Oct;33(13):1887–92.